# Molecular detection on a defective MoS_2 monolayer by simultaneous conductance and force simulations

Cesar Gonzalez Pascual, Y. J. Dappe

# Molecular detection on a defective $MoS_2$ monolayer by simultaneous conductance and force simulations

C. González[1,2,*] and Y. J. Dappe[3]

[1]*Departamento de Electrónica y Tecnología de Computadores, Campus de Fuente Nueva, Universidad de Granada, E-18071 Granada, Spain*

[2]*Departamento de Física Teórica de la Materia Condensada and Condensed Matter Physics Center (IFIMAC), Facultad de Ciencias, Universidad Autónoma de Madrid, E-28049 Madrid, Spain*

[3]*SPEC, CEA, CNRS, Université Paris-Saclay, CEA Saclay, 91191 Gif-sur-Yvette Cedex, France*

(Received 4 February 2017; revised manuscript received 17 May 2017; published 5 June 2017)

Based on simultaneous force and conductance simulations, a proof of concept for a potential method of molecular detection is presented. Using density functional theory calculations, a metallic tip has been approached to different small inorganic molecules such as CO, $CO_2$, $H_2O$, NO, $N_2$, or $O_2$. The molecules have been previously chemisorbed on a defect formed by two Mo atoms occupying a S divacancy on a $MoS_2$ monolayer where they are strongly bonded to the topmost substitutional molybdenum. At that site, the fixed molecules can be imaged by a conductive atomic-force-microscopy tip. Due to the differences in atomic composition and electronic configurations, each molecule yields specific conductance/force curves during the tip approach. A molecule-tip contact is established at the force minimum, followed by the formation of a characteristic plateau in the conductance in most of the cases. Focusing our attention on the position and values of such force minimum and conductance maximum, we can conclude that both characteristic properties can give a clear signature of each molecule, proposing a different method of detecting molecules adsorbed on highly reactive sites.

DOI: 10.1103/PhysRevB.95.214105

## I. INTRODUCTION

Transition-metal dichalcogenides have attracted great attention on both fundamental and technological levels. Among them, the most widely studied material is the molybdenum disulphide $MoS_2$. While the bulk phase exhibits a semiconductor character with an indirect gap, the single layer presents a direct gap [1–3]. This interesting and promising property can be exploited for applications in nanoelectronics, optoelectronics, spintronics, catalysis, and energy storage [4–11].

Two-dimensional (2D) materials are generally known as poorly reactive and, following this idea, many authors have fabricated transistors using $MoS_2$ monolayers in order to validate their potential application as gas-sensor devices [12–14]. Indeed, physisorbed molecules on a $MoS_2$ monolayer can modify its electronic properties and consequently the electronic current in the transistor is altered, leading to the molecular detection. The corresponding weak interaction has been theoretically evidenced for a wide range of small molecules on the perfect $MoS_2$ monolayer [15,16]. Most of them were physisorbed at a typical van der Waals (vdW) distance over the monolayer. For example, this weak interaction has been very recently confirmed in a study involving $CO_2$ molecules deposited on a $MoS_2$ monolayer [17]. Some molecules, such as NO or $NO_2$, experienced a stronger interaction with the monolayer [18], in good agreement with experimental evidence obtained in gas-sensing studies [12–14].

$MoS_2$ monolayers can be experimentally fabricated using different exfoliation techniques [4,19,20] or by chemical (CVD) and physical vapor deposition (PVD) [21–23]. Different kinds of defects can be produced during the growth process [24], leading to a change in the electronic, magnetic, or optical properties [22,25–27]. The defects can be classified into three types: point defects (such as vacancies or antisites), grain boundaries, and external borders of the compound. All of these imperfections seem to be very reactive, meaning that different atoms or molecules can be adsorbed or even dissociated [16,28–30]. Two good examples are the oxidation of the $MoS_2$ borders [28] and the sulfur vacancy self-healing using thiol molecules [29]. Even the molecular dissociation of $O_2$ molecules over $MoS_2$ defects has been shown very recently, both experimentally and theoretically [31,32].

Hong *et al.* demonstrated that the metallic defects formed by Mo substitutional atoms occupying the sulfur vacancies can be formed in the samples grown by the PVD technique [23]. We have recently shown, using the density functional theory (DFT) technique, that many small inorganic molecules such as CO, $CO_2$, $H_2O$, NO, $N_2$, or $O_2$ can be chemisorbed on these defects [16]. Based on atomic force microscopy (AFM), an alternative procedure for the molecular detection can be proposed. Indeed, AFM was suggested some years ago as a tool for chemical identification of the adsorbed elements on a semiconducting surface [33]. In a first step, the different $MoS_2$ defects should be found in the $MoS_2$ sample. For that purpose, AFM or scanning tunneling microscope (STM) images can show the characteristic fingerprint of each defect [30,34]. Then, unknown molecules can be deposited in the sample and will be strongly bonded to the metallic defects. In a final step, a conductive AFM tip can be approached to the selected sites, and standard force and conductance curves can be measured, determining the kind of molecule bonded to the defect.

In this work, we present a theoretical proof of concept for the detection of a molecule adsorbed on a $MoS_2$ metallic defect. Using DFT calculations, the force and conductance curves have been estimated approaching a Cu tip to different

*cesar.gonzalez.pascual@gmail.com

 

molecules such as CO, $CO_2$, $H_2O$, NO, $N_2$, or $O_2$ which are strongly bonded to the topmost Mo atom occupying a S divacancy in a $MoS_2$ monolayer. Our simulations show that the different force minima associated to the formation of a tip-molecule contact are directly linked to a characteristic conductance plateau obtained for each molecule. The performance of both simultaneous measurements and subsequent comparison to previous well-known results would allow the molecular detection of an unknown molecule with an scanning probe microscope (SPM).

## II. METHOD OF CALCULATION

All the structural relaxations have been performed using the DFT plane-wave Vienna Ab initio Simulation Package (VASP) code [35–37]. The Perdew-Burke-Ernzerhof (PBE) functional for the generalized gradient approximation (GGA) of the exchange and correlation potential [38] and the projector augmented wave (PAW) pseudopotentials [39] have been used in the simulations. Van der Waals (vdW) interactions have been included using the Grimme's parametrization implemented in VASP [40].

The atomic arrangement, electronic properties, and energetics of the system formed by different molecules adsorbed on a defective $6 \times 4$ rectangular unit cell of a $MoS_2$ monolayer have been previously investigated [16]. We demonstrated that the molecules CO, $CO_2$, NO, $O_2$, $H_2O$, and $N_2$ remained fixed on certain $MoS_2$ defects, such as two Mo atoms occupying a S divacancy. The molecules are bonded to one of the substitutional Mo atoms and the final structure presented a metallic character. In such work, we studied the stability of the molecules on this metallic defect with the temperature. For that purpose, we performed *ab initio* molecular dynamics (MD) calculations using the technique implemented in the FIREBALL code [41]. We demonstrated that only the $CO_2$ molecule was dissociated at room temperature, while the other molecules were stable at this defect. This molecule has been maintained on this work due to the potential measurement at lower temperatures where the $CO_2$ could be stable. The other molecules remained bonded to the Mo atom of the defect oscillating around the most stable position. The first movie of the Supplemental Material (SM) shows the *ab initio* MD simulation of a CO molecule adsorbed on the defective $MoS_2$ monolayer, showing such movement [42].

Over these initial structures, a Cu(111) tip formed by a pyramid of 35 atoms is approached to the molecules and both force and conductance curves are obtained from large to contact distances. This tip has been successfully used in many works before [30,43,44]. It is important to mention that we assume here a low reactive substrate underneath the defective $MoS_2$. The negligible effect on the electronic structure has been previously demonstrated theoretically [45] and experimentally [46]. For this reason, only the isolated monolayer is considered in our simulations.

The tip is positioned over the substitutional Mo atom as shown in Fig. 1(a) for the CO molecule case. The distance between the apex and the O atom of the molecule is initially fixed at 5 Å. The tip is rigidly approached by steps of 0.25 Å, as explained in a previous work [30]. For each step, the system is fully relaxed until the forces are lower than 0.025 eV/Å, using

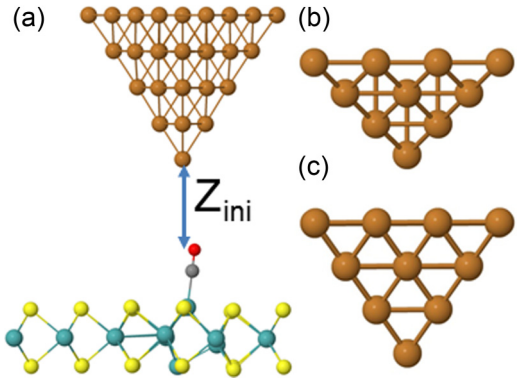


FIG. 1. (a) Atomic structure of the Cu(111)-rot0 tip (brown spheres) over a CO molecule (red/gray spheres) adsorbed on a defective $6 \times 4$ $MoS_2$ unit cell (yellow/blue spheres correspond to S/Mo atoms, respectively) at a distance of 5 Å (the defect is formed by two Mo substitutional atoms occupying a S divacancy). (b),(c) The alternative Cu(110) and Cu(100) tips, respectively.

an energy cutoff of 400 eV for the plane waves and 16 $k$ points in the first Brillouin zone (1BZ). Only the topmost layer of the tip and the lowest S atoms far away from the contact point are fixed at their initial positions. A vacuum layer was set to 12.0 Å in order to avoid interaction between neighboring cells in the perpendicular direction. After the relaxation, the mobile atoms are displaced from their original position in the initial system. The interaction between the tip and the substrate (in this study, the adsorbed molecule on the defective $MoS_2$ monolayer) changes with the tip approach. The tip-substrate force is estimated doing the derivative of the energetic curve obtained after the complete relaxation process. This curve can be directly compared to experimental measurements and its most representative point is the force minimum that corresponds to the strongest tip-substrate attraction.

In order to understand the effect of the tip on the force result, we have rotated by different angles (30, 60, and 90 degrees) the Cu(111) tip presented in Fig. 1(a) [from this point onwards, this tip will be denoted as Cu(111)-rot0]. Additionally, we have created two alternative Cu tips with (110) and (100) orientations as depicted in Figs. 1(b) and 1(c), respectively. In both cases, the metallic pyramid is formed by 30 atoms distributed in four layers. We have repeated, with these five additional tips, the same procedure previously explained.

For the conductance calculations, the Keldysh Green-function formalism implemented in the atomic-like orbital FIREBALL code has been used [41,47]. The values are presented in $G_0$ units (where $G_0 = 2e^2/h$ is the quantum of electrical conductance). In order to mimic the simultaneous force and conductance measurements, the atomic structures relaxed with VASP are fixed and the 1BZ has been sampled with 64 $k$ points. The electronic charges are estimated by the occupation of the atomic orbitals whose cutoff radii are shown in Table I. All of them have been extensively used in many previous works [16,48–50]. The methodology implemented in the FIREBALL package leads to overestimated bonding energies. For this reason, we used the plane-waves VASP code for the energetic-force estimation. For example, the adsorption energy of a CO molecule on the defective MoS2 monolayer is −1.95

TABLE I. Cutoff radii (in atomic units) used in the conductance calculation performed with the FIREBALL code [41]. The asterisk (*) indicates a double basis.

| | $r$ (a.u.) | | | | | | |
|---|---|---|---|---|---|---|---|
| Orbital | Mo | S | Cu | C | O* | N | H |
| *s* | 6.20 | 4.30 | 4.50 | 4.80 | 4.50 | 3.60 | 3.80 |
| *p* | 6.20 | 4.70 | 5.70 | 5.40 | 4.50 | 4.10 | |
| *d* | 5.80 | 5.50 | 3.70 | 5.20 | | 5.20 | |

and −2.39 eV with VASP and FIREBALL, respectively. On the other hand, FIREBALL has shown a great ability for the electronic transport simulations and a very good agreement with experimental results has been obtained in many different systems [43,44,47]. This combination of codes has been successfully exploited in previous works [43,51].

## III. RESULTS

We start with the analysis of a CO molecule adsorbed on the defect formed by two Mo atoms occupying a S divacancy on a $MoS_2$ layer [Fig. 1(a)]. The evolution of both force and conductance curves with the approach of the Cu(111)-rot0 tip is presented in Fig. 2(a). At large distances (5 Å), the tip-molecule interaction is mediated by weak electrostatic or vdW forces, resulting in a small amplitude in the force curve. The electronic transport lies in the tunneling regime and, consequently, a low conductance is also obtained [see Fig. 2(b)]. As the tip is approached, both attractive force and conductance slightly grow until the tip-O contact is formed around 2.75 Å, where a force minimum of −0.99 nN is found, as the filled squares curve shows in Fig. 2(a). The corresponding atomic structure is shown in Fig. 1(c). Beyond this point, the tip-O bond is maintained while the CO molecule rotates around the neighboring Mo atom. As a result, the force increases until it finds the repulsive regime at 1.25 Å. From this point onwards, the attractive force grows again (being more negative) due to the interaction between the tip and the C atom of the molecule [the atomic structure is shown in Fig. 2(d)]. The complete tip approach can be found in the second movie of the SM [42]. On the other hand, the contact formation is accompanied with a great jump in the conductance and the formation of a characteristic plateau with a value of 0.13 $G_0$. Several steps later, the conductance grows to 0.22 $G_0$ until the tip-C bond is formed.

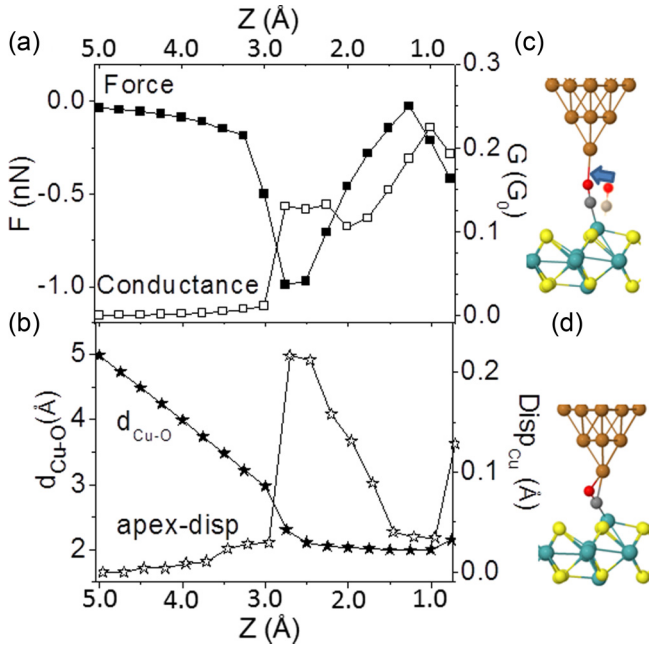


FIG. 2. (a) Force (filled black squares) and conductance (empty squares) curves calculated with the Cu(111)-rot0 tip over a CO molecule adsorbed on the selected $MoS_2$ defect. (b) Distance between the apex and the O atom in the molecule (filled black stars) and apex displacement (open stars) during the tip approach. The atomic structure of the tip Cu(111)-CO contact in (c) the force minimum and (d) at 1.0 Å.

These results can be correlated with the atomic rearrangements in the tip-molecule contact. In Fig. 2(b), the apex displacement from its ideal position in the unrelaxed tip (open stars) is presented for all the distances along the tip approach. An important jump in the contact formation is obtained similarly to the conductance curve. Moreover, the shape of the curve seems to be the opposite of the force curve, showing the direct relation between both force and conductance with the apex displacement. On the other hand, the apex-O distance (filled stars) shows a different behavior. Before the contact is formed, the apex-O distance decreases linearly with the tip approach, which is associated to the weak interaction and small atomic rearrangements. When the contact is established, the apex-O distance remains constant during the subsequent approach due to the molecular rotation around the Mo atom. The tip is retracted from the 1.25 Å point and the CO molecule remains bonded to the Mo atom in the defective $MoS_2$ layer (see the complete atomic movie in the SM [42]).

The increase of the attractive force and the conductance is reflected in a change in the molecular electronic structure. Figure 3 shows the density of states (DOS) of the CO molecule

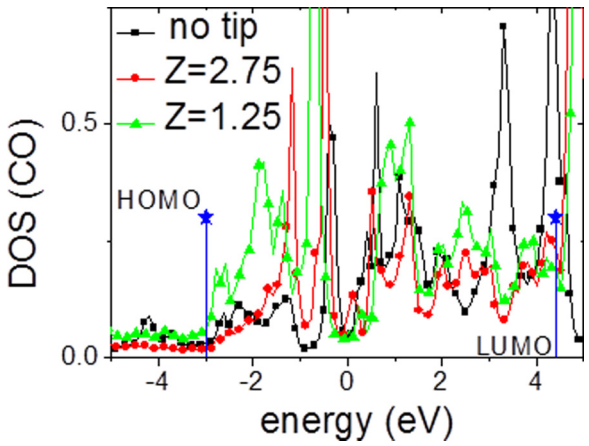


FIG. 3. Calculated DOS of the CO molecule bonded to one substitutional Mo atom in a S divacancy before the tip is approached (black squares), in the force minimum (red circles) and at the repulsive regime (green triangles). The blue stars represent the calculated HOMO and LUMO states of the isolated CO molecule.

bonded to the Mo substitutional atom for an infinite tip-CO distance (black squares) and the corresponding DOS for both interesting points: the force minimum (red circles) and at the repulsive regime (green triangles). The first curve clearly shows the almost symmetric bonding and antibonding states formed due to the molecule-Mo bond. Notice that the large gap obtained for the isolated molecule, defined by the energy difference between the highest occupied (HOMO) and the lowest unoccupied (LUMO) molecular orbitals (the blue stars in Fig. 3), is now full of new states due to the strong interaction with Mo atoms as presented in a previous work [16]. An appreciable change in the molecular states is observed at the contact point. Now, the minimum of the DOS obtained in the isolated case at the Fermi level is displaced to the occupied states area due to the tip-molecule charge transfer confirmed by our charge estimations. Before the tip approach, the molecule takes $0.10e^-$ from the metallic defect of the monolayer and, at the contact, it takes $0.20e^-$. An important DOS reconfiguration is obtained at the repulsive point, as shown in Fig. 3. In this case, the charge transfer on the molecule has slightly increased to $0.23e^-$.

In order to test the influence of the tip on the results, we have performed similar simulations using different Cu-based tips. In a first step, the initial Cu(111)-rot0 tip is rotated 30, 60, and 90 degrees. Second, we have used two additional Cu tips with different orientations, namely, (100) and (110). The corresponding force and conductance curves are collected in Figs. 4(a) and 4(b), respectively. We can observe that the values of both force and conductance have only slightly changed with the rotation of the Cu(111) tip and the different initial orientations. For example, the force has a value of −0.80 nN when the Cu(100) tip is used versus the −0.99 nN value of the Cu(111)-rot0 and the Cu(110) tips. In all the analyzed cases, the force minimum falls between 2.75 and 2.50 Å, and the displacements of both apex and molecule are similar, ranging from 0.18 to 0.30 Å and from 0.78 to 0.90 Å, respectively. The conductance curves, shown in Fig. 4(b), reflect the formation of the same regimes obtained with the Cu(111)-rot0 tip: a tunneling regime for large distances and the formation of a plateau when the apex-molecule contact is formed. Now, the values on the plateau range from 0.10 to 0.17 $G_0$. In the insets, we have included the atomic structure of the tip-CO contact for the Cu(111)-rot90 and Cu(100) tips in Figs. 4(a) and 4(b), respectively. Comparing both apex-CO contacts with the Cu(111)-rot0 case presented in Fig. 2(c), a similar configuration can be observed. All these results confirm that both force and conductance in the contact are mainly mediated by the bond formed between the tip apex and the O atom from the molecule. For a comparison with future experimental results, we can define both ranges of values in the force minimum and the conductance in the plateau instead of the single value obtained with the Cu(111)-rot0 (see Table III for details).

The same procedure can be applied to other molecules in order to compare the force minimum and the value at the conductance maximum for each case. These two parameters can be considered as the fingerprints of each molecule for a subsequent identification. Figure 5 shows the force and conductance curves calculated for different molecules probed by the Cu(111)-rot0 tip. It is important to mention that the tip is initially placed at the same position, fixed previously by the initial distance between the apex and the CO molecule.

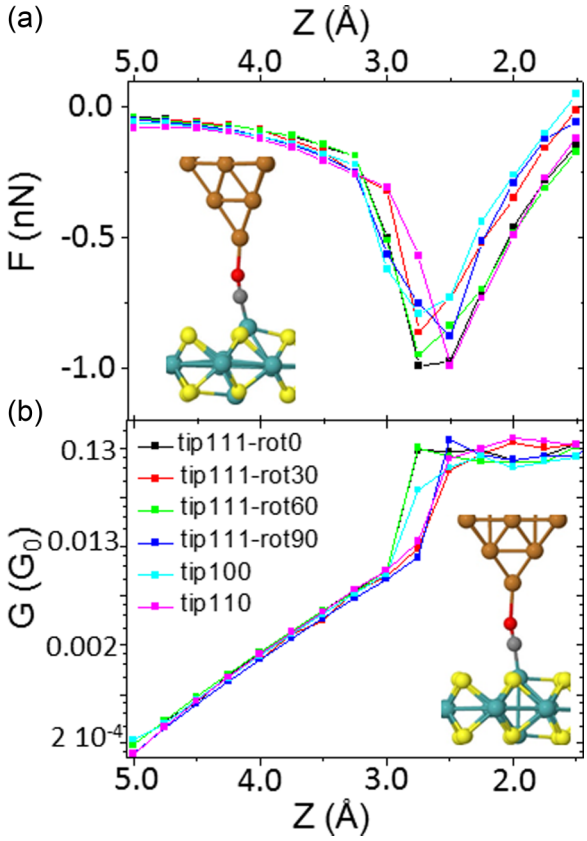


FIG. 4. Calculated (a) forces and (b) conductance (in logarithmic scale) for different tips approached to a CO molecule adsorbed on the defective $MoS_2$ monolayer: the initial Cu(111)-rot0 tip (black squares), the same tip rotated 30 (red squares), 60 (green squares), and 90 degrees (blue squares), a Cu(100) tip (light blue squares), and a Cu(110) tip (pink squares). Inset: Lateral view of the contact formed between the Cu(111)-rot90 tip (in the force graph) and the Cu(100) tip (in the conductance graph) with the CO molecule.

This can be an important issue because two molecules might present similar force minimum and a different position of such minimum can determine the molecular origin. In the experimental measurement, this initial distance can be fixed with the tunneling current or the position of the force minimum obtained on the pristine part of the monolayer.

The least interacting molecule is the $CO_2$ with a minimum force of −0.10 nN, the only case where no apex-molecule bond is formed, which justifies the low attraction [see the left inset of Fig. 5(a)]. If the tip is approached 1.0 Å more, a larger second minimum (of −0.23 nN) is obtained and, finally, a Cu-C bond is formed [see the right inset of Fig. 5(a)]. On the other hand, the other five molecules (including the previously analyzed CO) present a tip-molecule bond in the contact. In Figs. 5(c)–5(e) and the inset in Fig. 5(b), the atomic structure at the point of minimum force is shown for $N_2$, $O_2$, NO, and $H_2O$, respectively. The largest force is obtained on the $N_2$ molecule (−1.6 nN), while the $H_2O$ presents a much lower attraction (−0.48 nN). The contact formation is accompanied by a molecular displacement ($D_{mol}$) which is larger for the $N_2$ molecule (0.89 Å) and shorter for $H_2O$ with a corresponding value of 0.15 Å (see the values in the Table II).

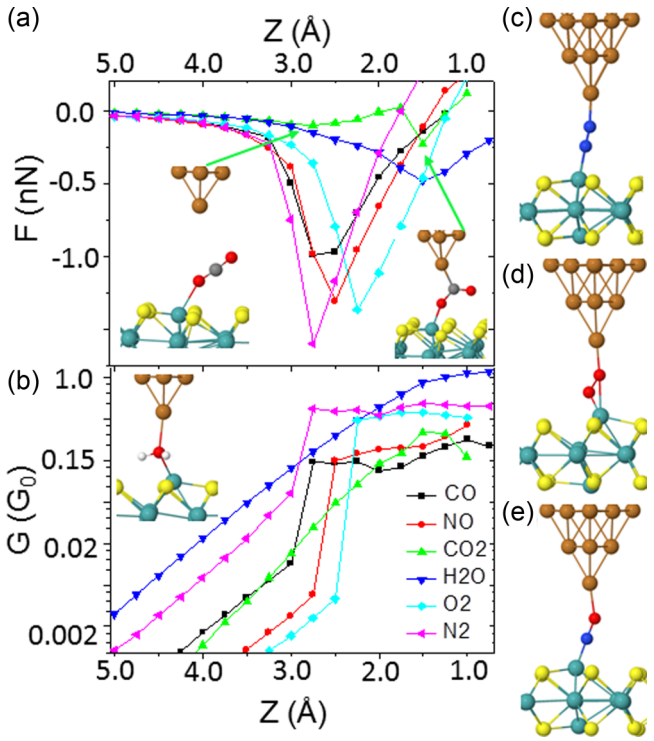


FIG. 5. Calculated (a) forces and (b) conductance (in logarithmic scale) for different molecules adsorbed on the defective $MoS_2$ monolayer: CO (black squares), NO (red circles), $CO_2$ (green up-triangles), $H_2O$ (blue down-triangles), $O_2$ (light-blue rhombus), and $N_2$ (pink left-triangles). Lateral view of the contact formed between the Cu tip (brown spheres) and the different molecules: (c) $N_2$, (d) $O_2$, and (e) NO molecules. Inset: The atomic configuration corresponding to both minima of the force in the $CO_2$ case and the $H_2O$ molecule. The light-blue, yellow, dark-blue, red, and white spheres correspond to Mo, S, N, O, and H, respectively.

In a previous work, we associated the apex displacement with the reactivity of the $MoS_2$ defect probed [30]. The present results seem to corroborate this general trend. The other two molecules NO and $O_2$ have very similar minimum forces ($-1.31$ and $-1.37$ nN, respectively). For this reason, a second parameter is required in order to determine the molecular origin. This constitutes an improvement in molecular detection with respect to the method presented before, where only the force was taken into account for the atomic identification [33].

The second fingerprint is the characteristic plateau or maximum conductance value obtained for each molecule when the contact is formed. The values obtained with the Cu(111)-rot0 tip are summarized in Table II and the curves are shown in Fig. 5(b). In this case, the largest conductance (1.1 $G_0$) is obtained for the $H_2O$ molecule. The curve increases monotonically until the maximum value is found. A similar behavior is obtained for the other triatomic molecule, $CO_2$. In this case, the conductance grows to 0.26 $G_0$ and the maximum is found close to the second minimum on the force. On the other hand, the diatomic molecules present two clearly different regimes in the curves: the tunneling regime for large distances where the conductance grows exponentially [see the linear increase in the logarithmic scale of Fig. 5(b)] and the contact regime where a plateau is formed after the jump associated to the contact formation and a great molecular displacement (see the values in Table II). These molecules can be divided into two subgroups: the homonuclear diatomic $N_2$ and $O_2$ molecules present similar conductance values in the plateau (around 0.47 and 0.42 $G_0$), whereas heteronuclear diatomic NO and CO molecules exhibit a much lower conductance plateau (around 0.18 and 0.13 $G_0$, respectively). Therefore, the conductance is a key parameter to distinguish $O_2$ and NO molecules.

We can repeat a similar analysis using the alternative tips previously presented: the Cu tips built with the (100) or (110) orientation and the Cu(111)-rot0 tip with different rotations. In all the cases, the apex starts the approaching process from the same initial point. From the results obtained when the family of Cu tips was applied on the CO molecule, we could conclude that the force minimum is (almost) found at the same distance because the force is mainly governed by the apex-molecule interaction in the contact regime. For this reason, we can expect only small changes in the most important parameters due to the different orientation and/or geometry of each tip. This is confirmed by the analysis of the Cu(100) tip presented in Fig. 6(a). The force minima maintain the same trend. First, the lowest interacting molecule is $CO_2$ that now gives a value of $-0.14$ nN. The second case is the water molecule ($-0.54$ nN) much closer to the CO molecule ($-0.79$ nN) than in the simulations performed with the Cu(111)-rot0 tip. Finally, the other three molecules present larger forces: $-1.60$ nN for $N_2$ and again with similar values NO ($-1.38$ nN) and $O_2$ ($-1.47$ nN).

TABLE II. Relevant variables for the Cu(111)-rot0 tip approaching to the different molecules adsorbed on the defective $MoS_2$ layer: apex/molecular displacement ($D_{apex/mol}$), charge transfer in the molecule [$\Delta C_{mol}(e)$], minimum force value ($F_m$), distance at which $F_m$ occurs ($Z_m$), and maximum of the conductance ($G_M$).

| Tip Cu(111)-rot0 | CO | NO | $H_2O$ | $N_2$ | $O_2$ | $CO_2$ |
|---|---|---|---|---|---|---|
| $D_{apex}$(Å) | 0.21 | 0.28 | 0.10 | 0.26 | 0.36 | 0.01 |
| $D_{mol}$(Å) | 0.86 | 0.66 | 0.15 | 0.89 | 0.73 | 0.12 |
| $\Delta C_{mol}(e)$ | 0.20 | 0.52 | 0.14 | 0.59 | 0.24 | 0.06 |
| $F_m$(nN) | $-0.99$ | $-1.31$ | $-0.48$ | $-1.60$ | $-1.37$ | $-0.10$ |
| $Z_m$(Å) | 2.75 | 2.50 | 1.50 | 2.75 | 2.25 | 2.75 |
| $G_M(G_0)$ | 0.13 | 0.18 | 1.10 | 0.47 | 0.42 | 0.26 |

## IV. DISCUSSION

From those results, a first conclusion can be established: the combination of force and conductance allows us to clearly distinguish all the molecules presented before if the same tip can be used in the test. For instance, using the Cu(111)-rot0 tip and considering only the minimum force value, we can clearly distinguish the poorly reactive $CO_2$ molecule, the low reactive $H_2O$ molecule, the moderately reactive CO, NO, and $O_2$, and the highly reactive $N_2$, when all of them are bonded to the $MoS_2$ defect formed by two substitutional Mo atoms occupying a S divacancy. It is important to notice that the force in this group of three diatomic molecules, with at least one O atom, increases with the number of electrons in the second atom (from the four electrons and $-0.99$ nN of C to the six

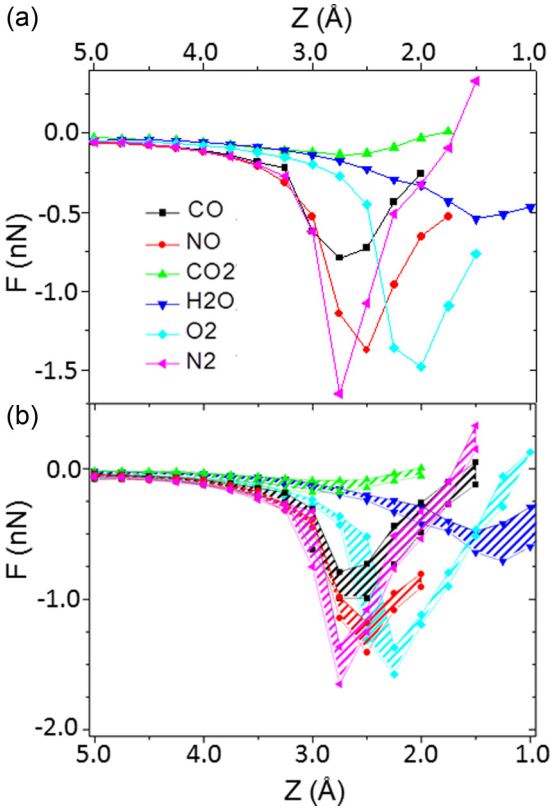


FIG. 6. Calculated (a) forces for different molecules adsorbed on the defective $MoS_2$ monolayer with a Cu(100) tip and (b) force ranges following the results obtained for all the Cu-based tips approached to the different molecules adsorbed on the defective $MoS_2$ monolayer: the black squares and area correspond to the CO molecule, while the red circles, green up-triangles, blue down-triangles, light-blue rhombus, and pink left-triangles and areas are attributed to the NO, $CO_2$, $H_2O$, $O_2$, and $N_2$, respectively.

electrons and −1.37 nN of O). Unfortunately, the NO and $O_2$ molecules could hardly be distinguished experimentally due to their similar shape and force minimum on the approach curve. This group of molecules, as well as the water one, were contacted by the tip forming an apex-O bond, but the obtained force minima present great differences in some of the cases, confirming the great influence of the environment that can dramatically change the electronic configuration of the O atom.

Following with the analysis of the forces, two additional general considerations can be drawn for molecules probed by the Cu(111)-rot0 AFM tip. First, there is an important geometrical consideration, which is that diatomic molecules present an almost vertical configuration, orthogonal to the $MoS_2$ plane, whereas triatomic molecules stand in a horizontal configuration parallel to the surface. These atomic arrangements lead to a much lower attraction over the triatomic molecules and smaller force minimum in the contact point. As a consequence, a tiny displacement is obtained on the triatomic molecules. This behavior should likely be studied for bigger planar molecules in order to find a generalization that could involve both the number of atoms in the molecule and the planar/perpendicular arrangement. Second, there is a preference of the tip to be bonded to an N atom better than an O one. This is in agreement with the preference of the NO molecule to bind to the Mo atom through the N atom [16].

On the electronic conductance side, the triatomic $H_2O$ and $CO_2$ present a monotonous increase until the maximum is obtained in the contact point. Interestingly, $H_2O$ produces the highest conductance (1.1 $G_0$), whereas it is much smaller over the $CO_2$ molecule. In the case of the $H_2O$ molecule, the contact is established through the oxygen atom, while at least two atoms are placed between the apex and the Mo atom in the other molecules. The effect of a single atom reduces the resistance in the contact, increasing the conductance. Regarding diatomic molecules, the conductance curves present a clear plateau at the contact regime. The group of three molecules with at least one O atom follows a similar order as the forces. Now the higher number of electrons in the second atom leads to a larger value of the conductance (0.42 $G_0$ for $O_2$ vs 0.13 $G_0$ for CO). Alternatively, we can separate the diatomic molecules into homonuclear and heteronuclear. The former type, $N_2$ and $O_2$, leads to larger conductances in the plateau than the latter type (NO and CO molecules), revealing a larger charge transfer to the symmetric molecules and a better coupling with both tip and $MoS_2$ defect. A general interpretation would require a deeper analysis of the electronic structure and electronegativity for a much larger number of molecules.

From the results previously presented, we can conclude that it is possible to clearly identify an unknown molecule if we are able to do the measurements with the same tip used in the reference test. Unfortunately, the geometry of the tip is hardly determined in an experimental measurement and two different tips can be created with different orientation or different rotational state, leading to slightly different force or conductance curves over the same point or molecule. Consequently, we should define some force/conductance ranges instead of a single value in order to characterize the molecules. For each one, the force curves can be collected in the same graph, as Fig. 4(a) shows for the CO case. An area can be defined between the maximum and minimum values of all the curves. The black area of Fig. 6(b) shows the force range defined from the force curves of the CO molecule. It is important to notice that the force minima is expected to take a value in the range mentioned before (−0.78 and −0.99 nN). A similar procedure can be followed with the other molecules. The corresponding areas are included in Fig. 6(b). We have associated to each molecule the same color and symbol as before, i.e., the red, green, blue, light-blue, and pink areas correspond to the NO, $CO_2$, $H_2O$, $O_2$, and $N_2$ molecules, respectively. In an experimental AFM measurement, we can expect that the force curve will fall within the corresponding area associated to each molecule when an unknown Cu tip is used. Interestingly, the results seem to maintain the same general trend as the one obtained with the Cu(111)-rot0 and Cu(100) tips. The first case is the low interacting $CO_2$ molecule (with a minimum between −0.09 and −0.18 nN). The second least interacting molecule is $H_2O$ with a minimum range of −0.48 to −0.70 nN. The third molecule is CO with a range between −0.79 and −0.99 nN. Finally, we can find the other three highly interacting molecules. Comparing the ranges created with the simulation of the different tips, the $N_2$ and $O_2$ molecules can hardly be distinguished if the force measurement of each molecule is performed with different Cu-based tips. They

TABLE III. Ranges of the relevant variables for a Cu tip approaching to the different molecules adsorbed on the defective $MoS_2$ layer: apex/molecular displacement ($D_{apex/mol}$), charge transfer in the molecule [$\Delta C_{mol}(e)$], minimum force value ($F_m$), distance at which $F_m$ occurs ($Z_m$), and maximum of the conductance ($G_M$).

| Tip Cu | CO | NO | $H_2O$ | $N_2$ | $O_2$ | $CO_2$ |
|---|---|---|---|---|---|---|
| $D_{apex}$(Å) | 0.18/0.30 | 0.28/0.37 | 0.10/0.14 | 0.35/0.49 | 0.41/0.48 | 0.01/0.04 |
| $D_{mol}$(Å) | 0.78/0.90 | 0.64/0.66 | 0.12/0.16 | 0.63/0.82 | 0.72/0.78 | 0.10/0.20 |
| $\Delta C_{mol}(e)$ | 0.16/0.20 | 0.47/0.53 | 0.14/0.16 | 0.50/0.59 | 0.25/0.24 | 0.04/0.02 |
| $F_m$(nN) | −0.79/−0.99 | −1.18/−1.40 | −0.48/−0.70 | −1.40/−1.65 | −1.37/−1.55 | −0.09/−0.18 |
| $Z_m$(Å) | 2.50/2.75 | 2.50 | 1.50/1.25 | 2.75 | 2.25 | 3.00/2.75 |
| $G_M$($G_0$) | 0.10/0.17 | 0.16/0.28 | 1.08/1.20 | 0.40/0.60 | 0.28/0.45 | 0.29/0.13 |

exhibit a range value of −1.40 to −1.65 nN and −1.37 to −1.55 nN for $N_2$ and $O_2$, respectively. Interestingly, the $O_2$ molecule has a lower coincident range with the NO molecule (−1.18 to −1.40 nN), while the Cu(111)-rot0 tip suggested a similar force value on these two last molecules.

On the other hand, the conductance ranges seem to generally follow the same trend and order shown by the first analyzed Cu(111)-rot0 tip (the values are summarized in Table III together with all the other interesting parameters involved in the apex-molecule contact). It is important to notice that the value of the conductance plateau in the case of $N_2$ has increased with respect to the value of the Cu(111)-rot0 tip, while it decreased in the case of $O_2$. The conductance changes from 0.40 to 0.60 $G_0$ and 0.28 to 0.42 $G_0$ for $N_2$ and $O_2$, respectively. These values imply that when the conductance measurement would be larger than 0.5 $G_0$, we can expect a $N_2$ molecule adsorbed on the defect.

In the case where both force and conductance would fall in the common ranges of $N_2$ and $O_2$ during the measurement, a third parameter can be considered for the molecular identification: the position of the minimum. While the $N_2$ molecule presents the minimum at 2.75 Å, the $O_2$ molecule forms the force minimum at a closer distance, namely, 2.25 Å. The relative position is (almost) independent of the Cu tip used. The force minimum of a S atom in a perfect $MoS_2$ area can be considered as a good reference. From a previous work, we demonstrated that this minimum can be formed 3.0 Å above the $MoS_2$ surface [30]. The initial position of the apex in the present calculations is around 7.5 Å above the topmost S atoms; consequently, the force minimum will be obtained 5.25 and 5.75 Å above the surface for the $O_2$ and $N_2$ molecules, respectively, i.e., 2.25 and 2.75 Å, respectively, to the force minimum of an ideal S atom. Then, the position of the force minimum can be an important parameter in the molecular identification.

## V. CONCLUSIONS

In summary, here we have proposed a potential way for molecular detection using a conductive sharp AFM tip. Different inorganic small molecules, such as CO, $CO_2$, $H_2O$, $N_2$, $O_2$, and NO, are chemisorbed on the metallic defect of the $MoS_2$ monolayer formed by two Mo atoms occupying a S divacancy. Then, a metallic tip can be approached to the molecule, obtaining two characteristic force and conductance curves. The diatomic $N_2$ presents the largest force, showing that the tip prefers to be bonded to N atoms instead of O atoms from the other molecules. The molecules arranged (almost) perpendicular to the monolayer present larger forces than the highly tilted $CO_2$ and $H_2O$ molecules. Comparing only the minimum of the forces for the molecules analyzed in this work, the conductance is required as a second parameter for the molecular detection. The largest conductance is obtained over the water molecule where only the O atom directly connects the tip with the Mo atom of the defective monolayer. While the conductance grows monotonically over the triatomic $CO_2$ and $H_2O$, the diatomic molecules present a great jump in the conductance before a plateau is formed on the contact regime. The homonuclear molecules ($O_2$ and $N_2$) show similar conductance and larger values than the one obtained on the NO and CO molecules, showing a preferential contact on the symmetric cases. Finally, we can conclude that both force minimum and conductance maximum (and, under some circumstances, the position of the force minimum) can be considered as the fingerprints that allow the identification of each molecule for a given tip used in the simulation or in further measurements.

## ACKNOWLEDGMENTS

The authors thankfully acknowledge the computer resources at Tirant and MareNostrum and the technical support provided by University of Valencia (UV) and Barcelona Supercomputing Center (Project No. QCM-2016-1-0024), and the Alhambra supercomputer facilities at the University of Granada. C.G. acknowledges financial support from the Junta de Andalucía and the European Commission under the Cofunding of the 7th Framework Program in the People Program through the Andalucia Talent Hub program and from the Spanish Ministry of Economy and Competitiveness, through The María de Maeztu Programme for Units of Excellence in R&D (Grant No. MDM-2014-0377).

[1] K. F. Mak, C. Lee, J. Hone, J. Shan, and T. F. Heinz, Atomically Thin $MoS_2$: A New Direct-Gap Semiconductor, Phys. Rev. Lett. **105**, 136805 (2010).

[2] A. Splendiani, L. Sun, Y. Zhang, T. Li, J. Kim, C.-Y. Chim, G. Galli, and F. Wang, Emerging photoluminescence in monolayer $MoS_2$, Nano Lett. **10**, 1271 (2010).

[3] A. Kumar and P. K. Ahluwalia, Electronic structure of transition metal dichalcogenides monolayers 1H-$MX_2$ ($M$ = Mo, W; $X$ = S, Se, Te) from ab initio theory: New direct band gap semiconductors, Eur. Phys. J. B **85**, 186 (2012).

[4] B. Radisavljevic *et al.*, Single-layer $MoS_2$ transistors, Nat. Nanotechnol. **6**, 147 (2011).

[5] J. Yoon *et al.*, Highly flexible and transparent multilayer $MoS_2$ transistors with graphene electrodes, Small **9**, 3185 (2013).

[6] Q. H. Wang, K. Kalantar-Zadeh, A. Kis, J. N. Coleman, and M. S. Strano, Electronics and optoelectronics of two-dimensional transition metal dichalcogenides, Nat. Nanotechnol. **7**, 699 (2012).

[7] R. R. Chianelli, G. Berhault, and B. Torres, Unsupported transition metal sulfide catalysts: 100 years of science and application, Catalysis Today **147**, 275 (2009).

[8] G. D. Du, Z. P. Guo, S. Q. Wang, R. Zeng, Z. X. Chen, and H. K. Liu, Superior stability and high capacity of restacked molybdenum disulfide as anode material for lithium ion batteries, Chem. Commun. **46**, 1106 (2010).

[9] S. G. Sørensen, H. G. Füchtbauer, A. K. Tuxen, A. S. Walton, and J. V. Lauritsen, Structure and electronic properties of in situ synthesized single-layer $MoS_2$ on a gold surface, ACS Nano **8**, 6788 (2014).

[10] X. Lu, M. I. B. Utama, J. Zhang, Y. Zhao, and Q. Xiong, Layer-by-layer thinning of $MoS_2$ by thermal annealing, Nanoscale **5**, 8904 (2013).

[11] L. Tao, H. Long, B. Zhou, S. F. Yu, S. P. Lau, Y. Chai, K. H. Fung, Y. H. Tsang, J. Yao, and D. Xu, Preparation and characterization of few-layer $MoS_2$ nanosheets and their good nonlinear optical responses in the PMMA matrix, Nanoscale **6**, 9713 (2014).

[12] H. Li, Z. Yin, Q. He, H. Li, X. Huang, G. Lu, D. W. H. Fam, A.-l. Y. Tok, Q. Zhang, and H. Zhang, Fabrication of single and multilayer $MoS_2$ film-based field-effect transistors for sensing NO at room temperature, Small **8**, 63 (2012).

[13] B. Liu, L. Chen, G. Liu, A. N. Abbas, M. Fathi, and C. Zhou, High-performance chemical sensing using Schottky-contacted chemical vapor deposition grown monolayer $MoS_2$ transistors, ACS Nano **8**, 5304 (2014).

[14] Q. Y. He, Z. Zeng, Z. Yin, H. Li, S. Wu, X. Huang, and H. Zhang, Fabrication of flexible $MoS_2$ thin-film transistor arrays for practical gas-sensing applications, Small **8**, 2994 (2012).

[15] S. Zhao, J. Xue, and W. Kang, Gas adsorption on $MoS_2$ monolayer from first-principles calculations, Chem. Phys. Lett. **595-596**, 35 (2014).

[16] C. González, B. Biel, and Y. J. Dappe, Adsorption of small inorganic molecules on a defective $MoS_2$ monolayer, Phys. Chem. Chem. Phys. **19**, 9485 (2017).

[17] Y. Qi, Q. Xu, Y. Wang, B. Yan, Y. Ren, and Z. Chen, $CO_2$-induced phase engineering: Protocol for enhanced photoelectrocatalytic performance of 2D $MoS_2$ nanosheets, ACS Nano **10**, 2903 (2016).

[18] Q. Yue, Z. Shao, S. Chang, and J. Li, Gas adsorption on $MoS_2$ monolayer from first-principles calculations, Nanoscale Res. Lett. **8**, 425 (2013).

[19] Z. Zeng, Z. Yin, X. Huang, H. Li, Q. He, G. Lu, F. Boey, and H. Zhang, Single-layer semiconducting nanosheets: High-yield preparation and device fabrication, Angew. Chem. **50**, 11093 (2011).

[20] S.-L. Zhang, H.-H. Choi, H.-Y. Yue, and W.-C. Yang, Controlled exfoliation of molybdenum disulfide for developing thin film humidity sensor, Curr. Appl. Phys. **14**, 264 (2014).

[21] S. Najmaei *et al.*, Vapour phase growth and grain boundary structure of molybdenum disulphide atomic layers, Nat. Mater. **12**, 754 (2013).

[22] J. Mann *et al.*, Facile growth of monolayer $MoS_2$ film areas on $SiO_2$, Eur. Phys. J. B **86**, 226 (2013).

[23] J. Jinhua Hong, Z. Hu, M. Probert, K. Li, D. Lv, X. Yang, L. Gu, N. Mao, Q. Feng, L. Xie *et al.*, Exploring atomic defects in molybdenum disulphide monolayers, Nat. Commun. **6**, 6293 (2015).

[24] W. Zhou, X. Zou, S. Najmaei, Z. Liu, Y. Shi, J. Kong, J. Lou, P. M. Ajayan, B. I. Yakobson, and J. C. Idrobo, Intrinsic structural defects in monolayer molybdenum disulfide, Nano Lett. **13**, 2615 (2013).

[25] M. V. Bollinger, J. V. Lauritsen, K. W. Jacobsen, J. K. Nørskov, S. Helveg, and F. Besenbacher, One-Dimensional Metallic Edge States in $MoS_2$, Phys. Rev. Lett. **87**, 196803 (2001).

[26] J. V. Lauritsen, J. Kibsgaard, G. H. Olesen, P. G. Moses, B. Hinnemann, S. Helveg, J. K. Nørskov, B. S. Clausen, H. Topsøe, E. Lægsgaard, Location and coordination of promoter atoms in Co- and Ni-promoted $MoS_2$-based hydrotreating catalysts, J. Catal. **249**, 220 (2007).

[27] Z. Zhang, X. Zou, V. H. Crespi, and B. I. Yakobson, Intrinsic magnetism of grain boundaries in two-dimensional metal dichalcogenides, ACS Nano **7**, 10475 (2013).

[28] R. Ionescu, A. George, I. Ruiz, Z. Favors, Z. Mutlu, C. Liu, K. Ahmed, R. Wu, J. S. Jeong, L. Zavala, K. A. Mkhoyan, M. Ozkanacd, and C. S. Ozkan, Oxygen etching of thick $MoS_2$ films, Chem. Commun. **50**, 11226 (2014).

[29] M. Makarova, Y. Okawa, and M. Aono, Selective adsorption of thiol molecules at sulfur vacancies on $MoS_2$(0001), followed by vacancy repair via S-C dissociation, J. Phys. Chem. C **116**, 22411 (2012).

[30] C. González, Y. J. Dappe, and B. Biel, Reactivity enhancement and fingerprints of point defects on a $MoS_2$ monolayer assessed by *ab initio* atomic force microscopy, J. Phys. Chem. C **120**, 17115 (2016).

[31] L. Qi, Y. Wang, L. Shen, and Y. Wu, Chemisorption-induced $n$-doping of $MoS_2$ by oxygen, Appl. Phys. Lett. **108**, 063103 (2016).

[32] B. Akdim, R. Pachter, and S. Mou, Theoretical analysis of the combined effects of sulfur vacancies and analyte adsorption on the electronic properties of singlelayer $MoS_2$, Nanotechnology **27**, 185701 (2016).

[33] Y. Sugimoto *et al.*, Chemical identification of individual surface atoms by atomic force microscopy, Nature (London) **446**, 64 (2007).

[34] C. González, B. Biel, and Y. J. Dappe, Theoretical characterisation of point defects on a $MoS_2$ monolayer by scanning tunnelling microscopy, Nanotechnology **27**, 105702 (2016).

[35] G. Kresse and J. Hafner, *Ab initio* molecular dynamics for liquid metals, Phys. Rev. B **47**, R558 (1993).

[36] G. Kresse and J. J. Furthmuller, Efficient iterative schemes for *ab initio* total-energy calculations using a plane-wave basis set, Phys. Rev. B **54**, 11169 (1996).

[37] G. Kresse and D. Joubert, From ultrasoft pseudopotentials to the projector augmented-wave method, Phys. Rev. B **59**, 1758 (1999).

[38] J. P. Perdew, K. Burke, and M. Ernzerhof, Generalized Gradient Approximation Made Simple, Phys. Rev. Lett. **77**, 3865 (1996).

[39] P. E. Blöchl, Projector augmented-wave method, Phys. Rev. B **50**, 17953 (1994).

[40] S. Grimme, Semiempirical GGA-type density functional constructed with a long-range dispersion correction, J. Comput. Chem. **27**, 1787 (2006).

[41] J. P. Lewis *et al.*, Advances and applications in the FIREBALL *ab initio* tight-binding molecular-dynamics formalism, Phys. Status Solidi B **248**, 1989 (2011).

[42] See Supplemental Material at http://link.aps.org/supplemental/10.1103/PhysRevB.95.214105 for a first movie showing the MD simulation at 300 K of a CO molecule adsorbed on a defective $MoS_2$ and a second movie showing the Cu tip approach (and retraction) to a CO molecule adsorbed on the defected $MoS_2$ monolayer.

[43] M. Ternes, C. González, C. P. Lutz, P. Hapala, F. J. Giessibl, P. Jelínek, and A. J. Heinrich, Interplay of Conductance, Force, and Structural Change in Metallic Point Contacts, Phys. Rev. Lett. **106**, 016802 (2011).

[44] G. Schull, Y. J. Dappe, C. González, H. Bulou, and R. Berndt, Charge injection through single and double carbon bonds, Nano Lett. **11**, 3142 (2011).

[45] K. Dolui, I. Rungger, C. D. Pemmaraju, and S. Sanvito, Possible doping strategies for $MoS_2$ monolayers: An *ab initio* study, Phys. Rev. B **88**, 075420 (2013).

[46] S. W. Han *et al.*, Band-gap transition induced by interlayer van der Waals interaction in $MoS_2$, Phys. Rev. B **84**, 045409 (2011).

[47] J. M. Blanco, C. González, P. Jelínek, J. Ortega, F. Flores, and R. Pérez, First-principles simulations of STM images: From tunneling to the contact regime, Phys. Rev. B **70**, 085405 (2004).

[48] D. Di Felice, E. Abad, C. González, A. Smogunov, and Y. J. Dappe, Angle dependence of the local electronic properties of the graphene/$MoS_2$ interface determined by ab initio calculations, J. Phys. D: Appl. Phys. **50**, 17LT02 (2017).

[49] G. Otero *et al.*, Fullerenes from aromatic precursors by surface-catalysed cyclodehydrogenation, Nature (London) **454**, 865 (2008).

[50] J. I. Martínez, E. Abad, C. González, F. Flores, and J. Ortega, Improvement of Scanning Tunneling Microscopy Resolution with H-Sensitized Tips, Phys. Rev. Lett. **108**, 246102 (2012).

[51] M. Ondráček, P. Pou, V. Rozsíval, C. González, P. Jelínek, and R. Pérez, Forces and Currents in Carbon Nanostructures: Are We Imaging Atoms? Phys. Rev. Lett. **106**, 176101 (2011).